Analytical asymptotic velocities in linear Richtmyer-Meshkov-like flows

F. Cobos Campos and J. G. Wouchuk*

E.T.S.I. Industriales, Instituto de Investigaciones Energéticas and CYTEMA, Universidad de Castilla-La Mancha, 13071 Ciudad Real, Spain

(Received 30 July 2014; published 14 November 2014)

An analytical model to study the perturbation flow that evolves between a rippled piston and a shock is presented. Two boundary conditions are considered: rigid and free surface. Any time a corrugated shock is launched inside a fluid, pressure, velocity, density, and vorticity perturbations are generated downstream. As the shock separates, the pressure field decays in time and a quiescent velocity field emerges in the space in front of the piston. Depending on the boundary conditions imposed at the driving piston, either tangential or normal velocity perturbations evolve asymptotically on its surface. The goal of this work is to present explicit analytical formulas to calculate the asymptotic velocities at the piston. This is done in the important physical limits of weak and strong shocks. An approximate formula for any shock strength is also discussed for both boundary conditions.

DOI: 10.1103/PhysRevE.90.053007 PACS number(s): 47.20.−k, 52.58.Hm, 52.50.Lp

I. INTRODUCTION

Shock waves have been studied for approximately the past 200 years, with contributions coming from mathematicians, engineers, and physicists alike [1]. During the past century, the field of shock waves has seen a renewed interest because of its capabilities of generating matter with extreme conditions of pressure and temperature with different substances in the gas, liquid, or solid phases. An important problem in this field concerns the dynamics of corrugated shocks and the corresponding flows that develop downstream. Rippled shocks have been studied in different contexts and environments since the middle of the past century [2–27]. Around 1950, A. E. Roberts [2] was the first person to study the dynamics of the flow induced by a two-dimensional corrugated shock front in planar geometry with an analytic model, using Laplace transforms. Some 20 years later, R. D. Richtmyer [3] studied the problem of a planar shock crossing the corrugated boundary between two ideal gases. He numerically solved the fluid equations in order to follow the normal velocity perturbations at the corrugated interface as a function of time. He showed that, in this class of problems, the fluid velocities (within the domain of validity of the linear theory), reached an asymptotic value when the shock separated from the contact surface a distance on the order of the perturbation wavelength. Almost simultaneously, E. E. Meshkov in the former Soviet Union [4] designed a series of experiments that confirmed, at least qualitatively, the previous theoretical predictions of Richtmyer. More or less at the same time, other researchers were also studying this type of flow with the aid of shock tubes, as, for example, in the works of Briscoe and Kovitz [5]. By the end of the 1990s, the flows generated behind corrugated shock waves (and also behind corrugated rarefaction waves) began to be called Richtmyer-Meshkov-like flows (RM) [6]. Because of the rippled shape of the shock surface, velocity, and pressure perturbations are created behind the wave which affect the whole fluid downstream. As a consequence, as the shock separates from the piston driving it, significant hydrodynamic perturbations are generated behind it which may drive the compressed fluid into a state of turbulence if it enters the nonlinear regime. This kind of flow occurs in many different contexts, ranging from laboratory-created experiments, as in the irradiation of inertial fusion targets, to natural environments like astrophysical events after the explosion of massive stars in the form of supernovas. Recently, the use of corrugated shock waves has been suggested as an important tool to diagnose material properties [7–9] within the domains of high-energy-density physics (HEDP) experiments or within the domain of geophysics or planetary sciences [10]. Therefore, analytical models that reveal the details of the linear phase are extremely important in order to develop consistent nonlinear theories of the perturbation evolution [11–13] or helping in the design of experiments [9] and/or assisting in the benchmarking of simulation hydrocodes dealing with RM-like flows. The work shown here is a natural extension of previous work on the subject [15,16] and the objective is very specific: to obtain accurate analytical estimates of the asymptotic velocities in an RM-like environment. The two simplest cases with a single fluid are studied: corrugated rigid piston and corrugated free surface. The free surface situation was for the first time analyzed within the context of RM-like flows in Ref. [17] and some years later it was studied again in Ref. [18] for the particular case in which the shock is infinitely strong and the fluid is extremely compressible. So far, no theoretical work has yet examined the dependence of the tangential and normal asymptotic velocities at the surface of the piston (be it a rigid or a free surface) as a function of the shock strength and fluid compressibility in the whole range. The aim of this work is to show the scalings of those velocities as a function of the shock Mach number and the fluid isentropic exponent. Even though the main equations to be used had already been obtained in a previous work [16], they have never been used to study in detail the problems posed here. These calculations would serve as a first step towards more ambitious calculations aimed at obtaining similar formulas to the asymptotic velocities in the general RM environment dealing with two fluids for any shock Mach number and arbitrary fluids compressibilities. We structure the work in the following manner: In Sec. II we briefly review the linearized equations of motion in the space between a piston and a corrugated shock. They are necessary to settle the notation

*gustavo.wouchuk@uclm.es

used in the rest of the work. The pressure-wave equation is studied and the functional equation that governs the temporal evolution of the pressure perturbations is presented. In Sec. III the solutions for different boundary conditions at the piston are shown: rigid and free surfaces. We show the asymptotic velocities for different values of the shock Mach number and fluid compressibility. An approximate analytical formula and important scalings are obtained. In Sec. IV a brief summary is presented. The reader who is only interested in the final results may go directly to Sec. III. However, the notation and all the analytical ingredients necessary to assimilate those results are elaborated on with the corresponding depth in Sec. II.

II. LINEARIZED EQUATIONS

We consider an ideal gas with constant specific heat ratio γ, initial pressure p_1, and mass density ρ_1 bounded on the left by a planar surface that acts as a piston (Fig. 1). The piston starts to move at $t = 0$ to the right with speed $+U\hat{x}$ in the laboratory reference frame. A shock moving with speed D is launched in front of the piston. The pressure driving the shock is $p_2 > p_1$ and the density of the compressed fluid is $\rho_2 > \rho_1$. The sound speed in front of the shock is $c_1 = \sqrt{\gamma p_1/\rho_1}$. The compressed fluid sound velocity is $c_2 = \sqrt{\gamma p_2/\rho_2}$. The upstream shock Mach number is $M_1 = D/c_1 > 1$ and the downstream shock Mach number is $M_2 = (D-U)/c_2 < 1$.

A. Boundary conditions at the corrugated shock front

Compressed fluid quantities are connected with the upstream values through the Rankine-Hugoniot relationships (conservation of mass, momentum, and energy) [19]. We have, for the density ratio, the following:

$$R = \frac{\rho_2}{\rho_1} = \frac{D}{D-U} = \frac{(\gamma+1)M_1^2}{(\gamma-1)M_1^2+2}, \tag{1}$$

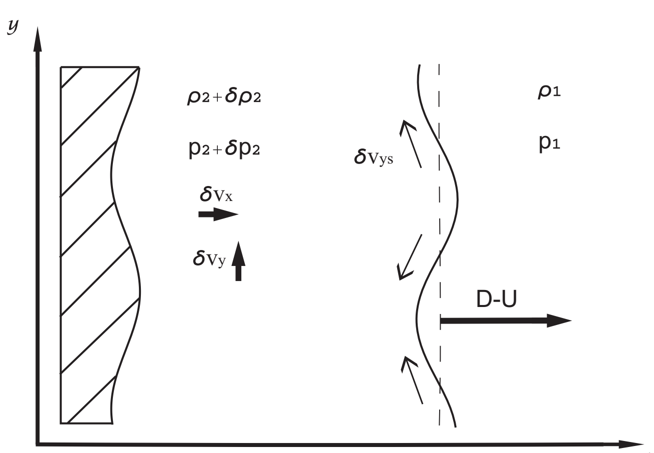

FIG. 1. A corrugated piston drives a rippled shock inside an ideal gas. The shock moves with speed $D-U$ in the piston reference frame. The downstream perturbations are indicated as well as the tangential velocity fluctuations just behind the shock (δv_{ys}).

and for the pressure ratio,

$$\frac{p_2}{p_1} = \frac{2\gamma M_1^2 - \gamma + 1}{\gamma+1}. \tag{2}$$

The ratio of sound velocities across the shock front is

$$\frac{c_2}{c_1} = \frac{\sqrt{\left(2\gamma M_1^2 - \gamma + 1\right)\left[(\gamma-1)M_1^2+2\right]}}{(\gamma+1)M_1}, \tag{3}$$

and the shock Mach number with respect to the compressed fluid is therefore

$$M_2 = \frac{D-U}{c_2} = \sqrt{\frac{(\gamma-1)M_1^2+2}{2\gamma M_1^2 - \gamma + 1}}. \tag{4}$$

The results shown in the previous equations relate the quantities at both sides of the shock wave assuming a planar shock, without perturbations and, as such, they serve us as background values. Our interest lies, however, in the situation in which the piston surface is slightly rippled with perturbation wavelength λ and an initial corrugation $\psi_0 \ll \lambda$. As discussed in Sec. I, the shock ripple will induce the generation of pressure and velocity perturbations in the space between the piston and the shock surface (see Fig. 1). We assume an initial piston corrugation of the form $\psi_p(0) = \psi_0 \cos ky$, where ψ_0 is the ripple amplitude and $k = 2\pi/\lambda$ is the perturbation wave number. From now on, we study the problem in a reference frame that moves with the piston. In the compressed fluid, perturbations in density ($\delta\rho$), velocity (δv_x and δv_y for the two components), and pressure (δp) are generated. We use the following definitions for the downstream perturbations:

$$\begin{aligned}
\frac{\delta\rho_2}{\rho_2} &= \tilde{\rho}(x,t)\cos ky,\\
\frac{\delta p_2}{\rho_2 c_2^2} &= \tilde{p}(x,t)\cos ky,\\
\frac{\delta v_x}{c_2} &= \tilde{v}_x(x,t)\cos ky,\\
\frac{\delta v_y}{c_2} &= \tilde{v}_y(x,t)\sin ky.
\end{aligned} \tag{5}$$

The normalizations defined above are best suited for solving the pressure-wave equation with the formalism presented here. However, when analyzing the asymptotic velocities at the piston, it will be useful to change the units of velocity. Each situation will be discussed accordingly in Sec. III.

The shock corrugation is a function of time and of the transverse coordinate: $\Psi_s(y,t) = \psi_s(t)\cos ky$. The dimensionless shock ripple amplitude is $\xi_s(t) = k\psi_s(t)$. It is clear that at $t = 0$, the initial shock ripple amplitude coincides with the piston corrugation amplitude. That is, $\psi_s(t=0) = \psi_0$. We define a dimensionless time $\tau = kc_2 t$. The different perturbed quantities just behind the shock front are related with each other through the conservation equations across the shock. Linearizing the conservation equations for mass, x momentum, y momentum, and energy, we arrive at the following relationships just behind the corrugated front [3,20]:

$$\frac{d\xi_s}{d\tau} = A_s \tilde{p}_s, \quad A_s = \frac{R}{R-1}\frac{M_1^2-1}{2M_1^2 M_2}, \tag{6}$$

$$\tilde{v}_{xs} = A_x \tilde{p}_s, \quad A_x = \frac{M_1^2+1}{2M_1^2 M_2}, \tag{7}$$

$$\tilde{\rho}_s = A_\rho \tilde{p}_s, \quad A_\rho = \frac{1}{M_1^2 M_2^2}, \tag{8}$$

$$\tilde{v}_{ys} = A_y \xi_s, \quad A_y = M_2(R-1). \tag{9}$$

An index "s" is always used to indicate that the quantity is evaluated at the shock front position, as in $\tilde{v}_{ys}$, and so on.

B. Linearized fluid equations: Pressure-wave equation

At first, we write the linearized versions of the fluid equations in the compressed fluid. We define the dimensionless space coordinates as follows: $\tilde{x} = ky$, $\tilde{y} = ky$. The mass conservation equation reads as follows:

$$\frac{\partial \tilde{\rho}}{\partial \tau} = -\frac{\partial \tilde{v}_x}{\partial \tilde{x}} - \tilde{v}_y. \tag{10}$$

The normal $\hat{x}$-direction and tangential $\hat{y}$-direction momentum equations are, respectively,

$$\frac{\partial \tilde{v}_x}{\partial \tau} = -\frac{\partial \tilde{p}}{\partial \tilde{x}}, \tag{11}$$

$$\frac{\partial \tilde{v}_y}{\partial \tau} = \tilde{p}. \tag{12}$$

Finally, the energy equation reduces to the conservation of entropy on the compressed fluid particles, as we assume an adiabatic flow between piston and shock. The only source of entropy perturbations lies at the shock surface. But once entropy is generated, it remains frozen to the fluid elements. In the reference frame used here, this condition leads us to the following familiar relationship:

$$\frac{\partial \tilde{p}}{\partial \tau} = \frac{\partial \tilde{\rho}}{\partial \tau}. \tag{13}$$

The above equations can be recast into the familiar two-dimensional (2D) wave equation for the pressure,

$$\frac{\partial^2 \tilde{p}}{\partial \tau^2} = \frac{\partial^2 \tilde{p}}{\partial \tilde{x}^2} - \tilde{p}. \tag{14}$$

The wave equation [Eq. (14)] has been solved in the recent past in the context of the RM instability and in the interaction of isolated shock fronts with upstream turbulent flows with the aid of a very useful coordinate transformation [5,16,20–22]. We define the variables r and χ as follows:

$$\begin{aligned} \tilde{x} &= r \sinh \chi, \\ \tau &= r \cosh \chi. \end{aligned} \tag{15}$$

Surfaces with $\chi = \text{const}$ represent planar fronts moving behind the shock following the trajectory $\tilde{x} = \tau \tanh \chi$. All the χ surfaces start to move at $\tau = 0$ and spread as time evolves. The shock front coordinate is defined by $\tanh \chi_s = M_2$. At the shock front, the value of $r = r_s$ is equal to $\tau\sqrt{1-M_2^2}$. After some long algebra, the wave equation inside the compressed fluid [Eq. (14)] can be rewritten in terms of the new coordinates in the following convenient form [16,20]:

$$r\frac{\partial^2 \tilde{p}}{\partial r^2} + \frac{\partial \tilde{p}}{\partial r} + r\tilde{p} = \frac{\partial \tilde{h}}{\partial \chi}, \tag{16}$$

where the auxiliar function $\tilde{h}$ is

$$\tilde{h} = \frac{1}{r}\frac{\partial \tilde{p}}{\partial \chi}. \tag{17}$$

Following the procedure described in Ref. [16] the wave equation can be reduced to a functional equation in the domain of the Laplace variable s of the Laplace transform theory. To this end, we define for any quantity $\phi(\chi,r)$ its Laplace transform (which will be indicated with capital letters) as

$$\Phi(\chi,s) = \int_0^\infty \phi(\chi,r)\exp(-sr)\,dr. \tag{18}$$

Thus, after some algebra, and making the variable change $s = \sinh q$, Eqs. (16) and (17) can be rewritten as follows:

$$\begin{aligned} \frac{\partial}{\partial q}(\cosh q\ \tilde{P}) + \frac{\partial \tilde{H}}{\partial \chi} &= 0, \\ \frac{\partial}{\partial \chi}(\cosh q\ \tilde{P}) + \frac{\partial \tilde{H}}{\partial q} &= 0. \end{aligned} \tag{19}$$

Integration of the last equation by changing to the auxiliary variables $q+\chi$ and $q-\chi$ leads us to the following decomposition for the perturbations $\tilde{P}$ and $\tilde{H}$:

$$\begin{aligned} \tilde{P}(\chi,q) &= \frac{F_1(q-\chi)+F_2(q+\chi)}{\cosh q}, \\ \tilde{H}(\chi,q) &= F_1(q-\chi) - F_2(q+\chi), \end{aligned} \tag{20}$$

where F_1 and F_2 are functions to be determined with the boundary conditions at the shock and at the piston surface. In the next subsection we write the appropriate form of the RH boundary conditions at the shock in terms of the new variables q and χ.

C. Laplace transform of the shock boundary conditions

In Ref. [3], Richtmyer combined Eqs. (7)–(9) into a pair of first-order partial differential equations coupling the shock ripple amplitude and the pressure perturbation behind the shock front. The procedure is straightforward: We take the total time derivative of Eq. (7) following the shock trajectory and combine it with the remaining equations to obtain the following:

$$-(M_2 + A_x)\frac{\partial \tilde{p}}{\partial \tau} = (1 + M_2 A_x)\frac{\partial \tilde{p}}{\partial \tilde{x}} + M_2 A_y \xi_s. \tag{21}$$

The last equation is coupled to Eq. (6). The Laplace transform of Eqs. (6) and (21) are written in the domain of the variable q as

$$\begin{aligned} \Xi_s(q) &= \frac{\xi_{s0} + A_s \cosh \chi_s \tilde{P}_s(q)}{\sinh q}, \\ \tilde{H}_s(q) &= -A_x \sinh q\ \tilde{P}_s(q) - M_2 A_y \cosh \chi_s\ \Xi_s(q). \end{aligned} \tag{22}$$

The function $\Xi_s(q)$ is the Laplace transform of the dimensionless ripple corrugation $\xi_s(r_s)$. In addition, the initial value of the pressure perturbation at the shock has been taken as $\tilde{p}_{s0} = 0$.

In the cases of interest here, the shock surface and the piston are infinitely near at $t = 0$ and it is reasonable to assume that $\tilde{p}_{s0} = 0$ [3]. As the piston has an initial corrugation, the value of $\psi_s(0) \neq 0$ coincides with the piston corrugation at $t = 0$. We have defined $\xi_{s0} = k\psi_0$. After some additional algebra, the last two equations can be solved for the shock pressure perturbations as [16,22]

$$\tilde{H}_s(q) = \alpha_1(q)\tilde{P}_s(q) + \alpha_2(q), \tag{23}$$

where

$$\alpha_1(q) = \alpha_{10}\sinh q + \frac{\alpha_{11}}{\sinh q}, \quad \alpha_2(q) = \frac{\alpha_{20}}{\sinh q}, \tag{24}$$

$$\begin{aligned} \alpha_{10} &= -A_x = -\frac{M_1^2+1}{2M_1^2 M_2}, \\ \alpha_{11} &= -\frac{1}{2M_2}, \\ \alpha_{20} &= -A_y\xi_{s0}\sinh\chi_s. \end{aligned} \tag{25}$$

It is noted that, in the above equation, α_{20} is proportional to the initial tangential velocity created behind the shock at $t = 0$: $\tilde{v}_{s0} = A_y\xi_{s0}$.

D. Boundary conditions at the piston surface and functional equations for the shock pressure perturbations

1. Rigid piston

Equation (23) relates the pressure perturbations $\tilde{H}_s$ and $\tilde{P}_s$, which is equivalent to relate the auxiliary functions F_1 and F_2, presented in Eq. (20). Which set of unknown functions to use is a matter of taste or convenience. In order to express the boundary conditions at the piston ($x = 0$), it will be convenient to deal with F_1 and F_2. As discussed in Ref. [16], if the shock is driven by a rigid piston, the natural condition is that the normal velocity is zero at $x = 0$ for any value of the time t. When this is translated into the language of the χ, q variables, requiring the vanishing of the normal pressure gradient there, we get

$$F_1(q) = F_2(q) = F(q). \tag{26}$$

Using this information, and going back to Eq. (20), together with Eq. (24), we arrive after some calculations to the following functional equation for the function $\tilde{P}_s(q)$:

$$\tilde{P}_s(q) = \lambda_1(q) + \lambda_2(q)\tilde{P}_s(q + 2\chi_s), \tag{27}$$

where

$$\begin{aligned} \lambda_1(q) &= \frac{\alpha_2(q) + \alpha_2(q + 2\chi_s)}{\cosh q - \alpha_1(q)}, \\ \lambda_2(q) &= \frac{\cosh(q + 2\chi_s) + \alpha_1(q + 2\chi_s)}{\cosh q - \alpha_1(q)}. \end{aligned} \tag{28}$$

For an ideal gas equation of state (EOS), the denominator of $\lambda_{1,2}$ has no singularities in the complex plane, other than branch points at $s = \pm i$, where i is the imaginary unit. This peculiarity explains the late time decay of the pressure perturbations, as will be discussed in the next section. For other substances, with nonideal EOS, the previous functional equation and its solutions have been briefly studied in the context of spontaneous acoustic emission of sound waves [23]. The mathematical complexity of Eq. (27) has made it impossible, up to now, to get an exact analytic solution expressible in finite form, that is, a solution that involves only a finite number of terms. We can only show, as in Refs. [16,22,23], a solution given by the infinite series,

$$\tilde{P}_s(q) = \lambda_1(q) + \sum_{n=1}^{\infty}\lambda_1(q + 2n\chi_s)\prod_{j=0}^{n-1}\lambda_2(q + 2j\chi_s). \tag{29}$$

Equation (29) is a particular solution to Eq. (27). Besides, it can be easily shown that the solution of the homogeneous equation must be identically zero for an ideal gas EOS. Therefore, Eq. (29) is the correct solution of the functional equation. All the information about the perturbation fields (pressure, velocity, etc.) of the whole compressed fluid can be obtained from the above solution for $\tilde{P}_s$. Indeed, getting $\tilde{P}_s$ as a function of the Laplace variable q [or, equivalently, $\tilde{p}_s(\tau)$ in the domain of the real time τ after a standard Laplace inversion] gives us complete information on the shock perturbation dynamics. Furthermore, knowing $\tilde{P}_s$ at the shock front allows us to know $\tilde{P}$ at any other surface χ and hence in the whole fluid downstream. As will be seen below, not only information on the irrotational sound waves but also the exact information about the asymptotic, steady-state, rotational velocity fields is also contained inside $\tilde{P}_s$. Unfortunately, in order to get that amount of information, it is necessary to deal with the functional equation Eq. (27) above, which does not admit, to our knowledge, an exact solution expressible in finite terms. The particular solution shown in Eq. (29) and the iterative process described later are the only ways to analytically deal with it. No other solution, so far, except Eq. (29), can be shown at the moment. The number of factors that compose each of the products increase with the index inside the summation. In general, this should be important only for very critical situations at high compressions and with fluids with γ very near unity. Nevertheless, we can show approximate solutions to the functional equation, which provide us with very accurate results for the asymptotic velocities, even in situations where high compression effects dominate, at the expense of not approaching the boundary $\gamma = 1$ which would require the infinite terms in the sum.

2. Free surface

The free surface boundary condition in the context of RM-like flows was considered for the first time in Ref. [17] as a particular case of the Riemann problem in a fluid. This situation can be handled also within the formalism presented here by choosing the appropriate relationship between the pressure auxiliary functions F_1 and F_2, as briefly discussed in Ref. [16]. The boundary condition at $x = 0$ consists in requiring the vanishing of the piston pressure fluctuations: $\tilde{p}(x = 0, t) = 0$. In the language of the variables χ, q, this is fulfilled if we require

$$F_1(q) = -F_2(q) = F(q). \tag{30}$$

Correspondingly, the shock pressure perturbations Laplace transform also satisfies a functional equation, identical in form to Eq. (27) but with different functions λ_1 and λ_2. We write below the corresponding functions $\lambda_{1,2}$ that guarantee the free surface boundary condition as follows (we correct here a typo in Eq. (44) of Ref. [16]):

$$\lambda_1(q) = \frac{\alpha_2(q) - \alpha_2(q+2\chi_s)}{\cosh q - \alpha_1(q)},$$
$$\lambda_2(q) = -\frac{\cosh(q+2\chi_s) + \alpha_1(q+2\chi_s)}{\cosh q - \alpha_1(q)}. \tag{31}$$

E. Useful approximations to Eq. (27)

Certainly Eq. (29) is the only exact solution known to date for Eq. (27). Its predictions have been compared successfully with the results of the linear simulations of Ref. [24] some time ago [16]. However, as it is expressed by an infinite series of very complicated terms (an iterative process to get its value is also possible, see Ref. [16]), it is much more convenient to have approximate analytical expressions that are easier to handle, valid at least in different limits of physical relevance: weak or strong shocks or high compression limits. The discussion that follows is general and holds for both boundary conditions at the piston. We start with the weak shock regime.

1. Weak shock limit

We need an expression for $\tilde{P}_s(q = \chi_s)$. It is not difficult to see that the solution to Eq. (27) can always be formally expanded as a Laurent series in powers of $s = \sinh q$ in the following form:

$$\tilde{P}_s(q) = \frac{\tilde{p}_{s1}}{s^2} + \frac{\tilde{p}_{s3}}{s^4} + \frac{\tilde{p}_{s5}}{s^6} + O\left(\frac{1}{s^8}\right), \tag{32}$$

for arbitrarily large values of $s = \sinh q$. The coefficient $\tilde{p}_{s1}$ is essentially the first time derivative of $\tilde{p}_s(r_s)$ as a function of the dimensionless time r_s and the other coefficients will be related to higher-order time derivatives of the shock pressure perturbations at $t = 0+$. The values of $\tilde{p}_{s1}$, $\tilde{p}_{s3}$, and $\tilde{p}_{s5}$ ... can be obtained by direct substitution inside Eq. (27) and equating equal powers of $1/s$. Once we have them, we substitute $s = \sinh \chi_s$ into the last equation above to obtain the value of $\tilde{P}_s(\chi_s)$. The resulting expression has to be expanded in powers of $M_1 - 1$ and we get the desired formula in the weak shock limit. This will be done in the next section when studying the asymptotic velocities. The number of coefficients that must be included in each case depends on the order of accuracy we want to achieve with this particular expansion. Retaining only the first coefficient ($\tilde{p}_{s1}$) gives a result that is accurate to the third order in $M_1 - 1$ (for the rigid piston asymptotic tangential velocity). Retaining the following term will give a result which is accurate up to the fourth order and so on. For the free surface, instead, it will be seen that the first coefficient gives an asymptotic velocity which is accurate only up to first order in $M_1 - 1$. Retaining $\tilde{p}_{s3}$ will be accurate up to second order and so on. Getting $\tilde{p}_{sj}$ for larger values of index j is tedious and not useful, because $1/\sinh \chi_s$ increases fast when the shock Mach number increases. Expansions like Eq. (32) are useful inside their circle of convergence which might decrease very fast for moderate to strong shocks. Those limited expansions are useful only for very weak shocks. As we cannot easily get the general term p_{sj} in analytical form in order to apply usual convergence tests, we can only compare the prediction of the first few terms with the exact solution obtained from the functional equation. As a general rule, we see that the expansion shown in Eq. (32) is good up to $M_1 \approx 1.4$. Adding a few more terms would not increase accuracy significantly because of the very slow speed of convergence.

2. Strong shock limit

The expansion used in Eq. (32) is good for weak shocks, because integer powers of $1/\sinh \chi_s$ become very small in this regime. The expansion shown in Eq. (32) is not practical for stronger shocks (typically $M_1 \geqslant 1.5$). We can circumvent this difficulty by solving the functional equation in an approximate way by iterating it one time, as was done numerically in Ref. [16]. The iterated solution then may be expanded analytically in powers of $1/M_1$ for sufficiently strong shocks and the solution thus obtained compared with the complete solution given by the whole series implied in Eq. (29). The idea was proposed in Ref. [16], even though it was never used to get approximate analytical estimates in this limit. We first solve Eq. (27) for $q \gg \chi_s$ and obtain a seed function $\tilde{P}_s^{[0]}(q)$ as follows:

$$\tilde{P}_s^{[0]}(q) = \frac{\lambda_1(q)}{1 - \lambda_2(q)}, \tag{33}$$

and iterate upon it, using Eq. (27), thus getting an improved estimate of the pressure as follows:

$$\tilde{P}_s^{[1]}(q) = \lambda_1(q) + \lambda_2(q)\tilde{P}_s^{[0]}(q + 2\chi_s). \tag{34}$$

This approximate choice gives enough accuracy for strong shocks if γ is not very near unity. If the fluid becomes very compressible, more iterations will be needed, because in that limit, sound reverberations are more important, which is manifested here in a significant number of shifts inside the argument of $\tilde{P}_s$. When evaluating the asymptotic velocity at the piston surface, we only need to substitute $q = \chi_s$ inside the result given in Eq. (34) above and expand in powers of $1/M_1$. This procedure will be done in the next section when studying the rigid piston and free surface asymptotic velocities separately.

F. Vorticity generated by the corrugated shock front

As the corrugated shock starts to move inside the fluid, tangential momentum must be conserved at both sides of the shock wave [19]. Because of this, a tangential velocity perturbation is created just behind the shock, according to Eq. (9) [3]. As discussed in previous works [16,20], the velocity field behind the shock is the superposition of two different fields: an irrotational part, created by the pressure gradients radiated in the form of sound waves downstream, and a rotational part, only created at the shock, due to the conservation of the tangential velocity. In fact, the amount of vorticity created at the corrugated shock can be easily calculated taking into account this fact. The details are the same whether the shock is isolated, as in Ref. [20], or not, as is the case here. We briefly review the derivation of the vorticity profile in order to settle the notation to be used in the next section. In a planar problem we are only concerned with the $\hat{z}$ component of the vorticity. The $\hat{z}$ component of the vorticity is defined by the following:

$$\delta\omega = \frac{\partial \delta v_y}{\partial x} - \frac{\partial \delta v_x}{\partial y},$$

which in dimensionless form is as follows:

$$\tilde{\omega} = \frac{\delta\omega}{kc_2} = \left(\frac{\partial \tilde{v}}{\partial \tilde{x}} + \tilde{u}\right)\sin ky. \tag{35}$$

Vorticity only can be generated behind the front. The second term in the right-hand side of the last equation ($\tilde{u}$) can be easily calculated by using Eq. (7). The first term has to be calculated from Eq. (9). To this scope, we take the total time derivative of Eq. (9) following the shock in its trajectory [15,20]. After some algebra, we get the final result,

$$\tilde{\omega} = g(\tilde{x})\sin ky, \;\; g(\tilde{x}) = \Omega\, \tilde{p}_s\left(r_s = \frac{\tilde{x}}{\sinh \chi_s}\right), \tag{36}$$

where it is seen that vorticity is only a function of the position of the particle and does not change in time (because no dissipative processes are assumed, in the absence of viscosity). Furthermore, the amount of vorticity generated at position x depends on the value of the shock pressure perturbation at the time the shock arrived to that position in space. The quantity Ω is dependent on the compressibility of the fluid and on the shock strength and can be seen to be equal to the following:

$$\Omega = A_x + \frac{A_y A_s - 1}{M_2} = \frac{\left(M_1^2 - 1\right)^2\sqrt{2\gamma M_1^2 - \gamma + 1}}{M_1^2\left[(\gamma-1)M_1^2 + 2\right]^{3/2}}. \tag{37}$$

As $\tilde{\omega}$ is not time dependent, the rotational velocity field associated to it does not depend on time either and is the only velocity perturbation that remains in the fluid when the shock moves very far from the piston. In fact, when the shock is still very near the piston surface, its ripple oscillates and radiates sound waves which modify the velocities. However, when the shock is very far, the pressure perturbations would have entered the asymptotic regime, becoming vanishingly small, and then the steady-state velocity profile emerges (given by the rotational part of the velocity field).

G. Velocity fields generated behind the corrugated fronts

After some algebra, the linearized equations of motion [Eqs. (10)–(12)] can be combined into wave equations for the velocity components as follows:

$$\begin{aligned}\frac{\partial^2 \tilde{v}_x}{\partial \tau^2} &= \frac{\partial^2 \tilde{v}_x}{\partial \tilde{x}^2} - \tilde{v}_x + g(\tilde{x}),\\ \frac{\partial^2 \tilde{v}_y}{\partial \tau^2} &= \frac{\partial^2 \tilde{v}_y}{\partial \tilde{x}^2} - \tilde{v}_y - g'(\tilde{x}),\end{aligned} \tag{38}$$

where $g'(\tilde{x})$ is an abbreviated form indicating the derivative $dg/d\tilde{x}$ in the last equation. As discussed in Ref. [20], the solution to the previous equations is the superposition of a rotational and an irrotational part,

$$\begin{aligned}\tilde{v}_x &= u_r(\tilde{x}) + u_{\rm irr}(\tilde{x},t),\\ \tilde{v}_y &= v_r(\tilde{x}) + v_{\rm irr}(\tilde{x},t).\end{aligned} \tag{39}$$

When the shock front is still near the piston, the influence of the pressure waves reverberating inside the fluid gives rise to the irrotational part of the velocity. As the shock separates and its distance to the piston is larger than a perturbation wavelength, the shock ripple decreases as does the pressure field. Hence, the irrotational velocities tend to zero and the steady state, asymptotic contribution (the rotational part) emerges. As discussed in Ref. [16], the late time velocity components satisfy the ordinary differential equations as follows:

$$\begin{aligned}\frac{d^2 u_r}{d\tilde{x}^2} - u_r &= -g(\tilde{x}),\\ \frac{d^2 v_r}{d\tilde{x}^2} - v_r &= g'(\tilde{x}).\end{aligned} \tag{40}$$

Both equations can be integrated with the Laplace transform technique, multiplying both sides by $\exp(-\sigma\tilde{x})$ and integrating in the interval $0 \leqslant \tilde{x} < \infty$. We only show the final result for the function u_r as follows:

$$U_r(\sigma) = \int_0^\infty u_r e^{-\sigma\tilde{x}}\, d\tilde{x} = \frac{\sigma u_p - v_p - \Omega \sinh\chi_s \tilde{P}_s(s = \sigma\sinh\chi_s)}{\sigma^2 - 1}, \tag{41}$$

where u_p is the normal velocity (for $t \to \infty$) and v_p is the asymptotic tangential velocity, both evaluated at the piston surface. An index "p" is always used to indicate that the corresponding quantity is evaluated at the piston surface. It is noted that $\tilde{P}_s(s = \sigma\sinh\chi_s)$ in Eq. (41) above is understood with $\tilde{P}_s$ as a function of the Laplace variable "s" and not of "$q = \sinh^{-1} s$." The main objective of this work is to characterize both piston velocities in the two cases of rigid and free surface boundary conditions. As the function u_r is finite everywhere, the Laplace transform U_r must be finite for $\sigma = 1$. This means that the numerator in the previous equation must vanish for $\sigma = 1$. Hence, the characteristic equation that determines the asymptotic velocities at the piston surface is equal to the following:

$$u_p - v_p = \Omega \sinh\chi_s \tilde{P}_s(q = \chi_s). \tag{42}$$

The equation above is the unique and exact contact surface boundary condition to be used in any RM-like problem when we want to determine the tangential and normal asymptotic velocities at the piston (or contact surface in the more general RM problem with two fluids). It becomes clear that both velocities are never independent of each other. For the boundary conditions considered in this work, their difference is proportional to an integral of the pressure perturbations at the shock front during its whole time history (or, equivalently, to a special space average of the vorticity profile generated by the shock). The value of $u_p - v_p$ is strongly influenced by the compressibility of the gas and the shock strength. Each case, rigid or free surface, deserves a separate discussion and the study of the previous equation for different values of γ and M_1 is done in the following section.

III. ASYMPTOTIC VELOCITIES: WEAK AND STRONG SHOCK LIMIT EXPANSIONS

Within the range of validity of the linear theory (that is, when the initial amplitude of the surface corrugation is very small compared to the corrugation wavelength), the conservation of tangential momentum across the shock is the mechanism responsible for generating tangential velocity perturbations behind the front which in turn drive a lateral mass flow [14]. This transverse mass flow is essential to create a modulated pressure perturbation profile just after the shock front which radiates downstream in the form of sound waves (see Fig. 1). These pressure fluctuations evolve in the whole fluid between the shock front and the piston thus inducing an irrotational velocity field everywhere, which is time and space dependent. Besides creating the sound-wave field, the conservation of tangential momentum across the shock wave is also responsible for generating vorticity. If viscosity is negligible, this vorticity field is conserved in the fluid elements and becomes an important ingredient to correctly describe the asymptotic evolution of the velocity field, even more so in the high-compression limit. In fact, as will be discussed later, vorticity generation is more important for strong shocks and for fluids with high compressibility. Then, as the shock travels farther from the piston surface, the velocity field that develops in the whole fluid downstream can be decomposed as the sum of an irrotational component (due to the fluid pressure fluctuations) and a rotational part (due to the vorticity created just behind the shock, that is, the divergence free perturbation mode commented in Refs. [13,14]). As is known, a shock moving inside an ideal gas is stable [23]; this means that pressure perturbations downstream of the shock will be zero for $t \to \infty$. The shock becomes planar after it has traveled several wavelengths from the piston. Therefore, asymptotically in time, as the shock regains its planar shape and the pressure field becomes vanishingly small, the fluid elements do not experience any more accelerations due to the sound waves and the asymptotic velocity field becomes steady. While the shock is still near the piston, the sound waves radiated by the shock reflect at the piston and go back to the shock surface. Thanks to this reflection, the shock knows about the conditions on the piston and, hence, consistently modifies the amount of vorticity that is being continuously generated. The process repeats itself as long as the shock travels away. We might expect a different kind of solution to the velocity field, depending on whether the piston is rigid. It is the main purpose of the work shown here to obtain analytical approximations to the asymptotic velocity field near the piston surface in two important kinds of RM-like flows inside ideal gases: when a shock is driven by a rigid piston and when it is driven by a free surface. Even though they are the simplest cases to be considered for a single shock moving inside a fluid, the mathematical details are cumbersome and, therefore, they need some explanation and will be provided later.

A. Rigid piston

For a rigid piston, we have $\delta v_x(x=0) \equiv \delta v_{xp} = 0$. Hence, we need only to determine the asymptotic tangential velocity at $x = 0$. From Eq. (42) we need the value of $\tilde{P}_s(q = \chi_s)$,

$$v_p = \left.\frac{\delta v_{yp}}{k\psi_0 c_2}\right|_{\tau\to\infty} = -\Omega \sinh \chi_s \tilde{P}_s(\chi_s), \tag{43}$$

where it is understood that $\delta v_{yp} \equiv \delta v_y(x=0)$. From dimensional arguments, we can always write the following relationship:

$$v_p = F(\gamma, p_1, p_2), \tag{44}$$

where the function F is an unknown function that must be obtained after solving the equations of motion with the boundary conditions. It is clear that F is dimensionless. Hence, according to the standard procedure in dealing with dimensional analysis [28], we can substitute it by a dimensionless function of dimensionless parameters. It is clear that p_2/p_1 is a function of γ, M_1. Hence, the governing dimensionless parameters are γ and M_1. Therefore, we write the previous relationship in the following form:

$$v_p = f(\gamma, M_1), \tag{45}$$

for some dimensionless function f. The exact calculation of f in the range $1 \leqslant M_1 < \infty$ for any value of γ can be accomplished by means of the infinite series provided by Eq. (29) and the definitions of Eq. (28). For weak shocks, the first term will be enough and as the shock strength increases, more terms are needed. In Fig. 2 we show δv_{yp} at the piston, in units of $k\psi_0 c_2$, as in Eq. (43) above. The infinite sum displayed in Eq. (29) has been used and the number of terms used was varied according to the values of M_1 and γ until four significant digits were assured. We would be tempted to assume complete similarity, as is usual in dimensional analysis [28], and eliminate, for example, the Mach number M_1 as an argument of the function f for very strong shocks and hence infer that the function f is only dependent on γ for $M_1 \gg 1$. The validity of this assumption can be confirmed by looking at Fig. 2 in the strong shock limit. In Fig. 3 we show the same

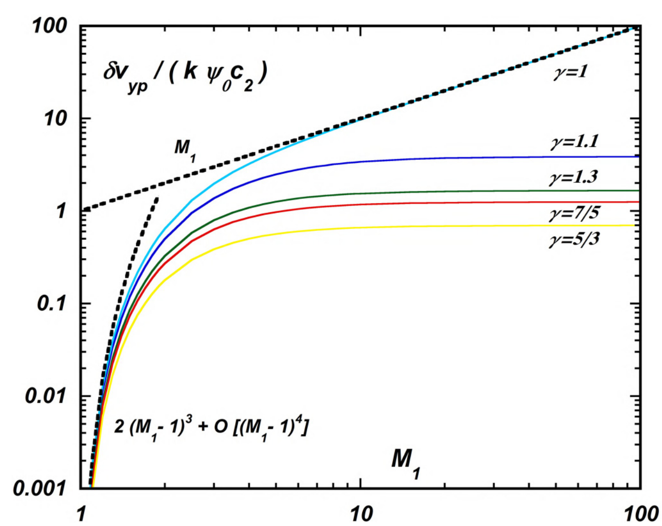

FIG. 2. (Color online) The tangential velocity δv_{yp} at the rigid piston surface when the shock is very far away as a function of the shock Mach number M_1 for different values of γ. The perturbation velocity is normalized in units of $k\psi_0 c_2$.

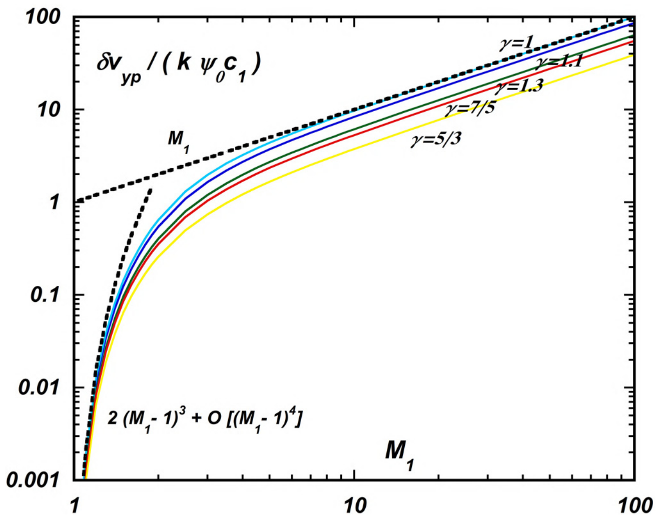

FIG. 3. (Color online) The tangential velocity δv_{yp} at the rigid piston surface when the shock is very far away as a function of the shock Mach number M_1 for different values of γ. The perturbation velocity is given in units of $k\psi_0 c_1$.

tangential velocity δv_{yp} as a function of M_1 for different values of γ but in units of $k\psi_0 c_1$. This requires us to multiply the result of Eq. (43) by the ratio c_2/c_1 given in Eq. (3). We see that all the curves are parallel straight lines for strong shocks in the logarithmic plot. This means that the dimensional velocity δv_{yp} is proportional to the shock speed D at high-enough values of M_1. The proportionality factor is dependent on the nature of the fluid and will be estimated soon below in the strong shock limit as a function of γ. In the following subsections, Eq. (43) will be studied in the different relevant physical limits of very weak and very strong shocks. The scaling seen in Fig. 3 at high values of M_1 can be easily deduced from the scaling obtained in Fig. 2. In fact, we have written above the following:

$$\left.\frac{\delta v_{yp}}{k\psi_0 c_2}\right|_{\tau\to\infty} = f(\gamma, M_1), \tag{46}$$

for some dimensionless function f. For very strong shocks, we know that $M_1 \gg 1$ is not a relevant parameter and hence

$$f(\gamma, M_1 \gg 1) \equiv g_1(\gamma), \tag{47}$$

for some dimensionless function g_1. Besides, it is easy to see from Eq. (3) that $c_2 \propto c_1 M_1$ in the strong shock limit. Therefore, upon substitution in the equations above, we get for the asymptotic velocity at the piston surface

$$\left.\frac{\delta v_{yp}}{c_2}\right|_{\tau\to\infty} < \left.\frac{\delta v_{yp}}{c_1}\right|_{\tau\to\infty} \propto M_1. \tag{48}$$

If $\gamma = 1$, from Eq. (3) we see that $c_2 = c_1$, which explains the behavior observed in Figs. 2 and 3.

1. Weak shock regime ($M_1 - 1 \ll 1$)

The weak shock limit is interesting, as it requires the simplest mathematical description and is more easily accessible in laboratory experiments [5]. For very weak shocks, we get from Eqs. (4), (15), and (37) the following:

$$\begin{aligned}\sinh\chi_s \cong{}& \frac{1}{\sqrt{2}\sqrt{M_1-1}} + \frac{(-5+3\gamma)\sqrt{M_1-1}}{4\sqrt{2}(\gamma+1)} \\ &- \frac{(21-38\gamma+5\gamma^2)(M_1-1)^{3/2}}{32(\sqrt{2}(\gamma+1)^2)} \\ &+ O[(M_1-1)^{5/2}], \\ \Omega \cong{}& \frac{4(M_1-1)^2}{\gamma+1} - \frac{8(\gamma-1)(M_1-1)^3}{(\gamma+1)^2} \\ &+ \frac{(29-30\gamma+5\gamma^2)(M_1-1)^4}{(\gamma+1)^3} + O[(M_1-1)^5].\end{aligned} \tag{49}$$

For the value of $\tilde{P}_s(\chi_s)$ we go to Eq. (32), substitute $s = \sinh\chi_s$, and use the coefficients $\tilde{p}_{s1}$, $\tilde{p}_{s3}$, and $\tilde{p}_{s5}$. These coefficients have to be obtained directly from the functional equation [Eq. (27)] and expand up to order 5 in powers of $M_1 - 1$. We only show the final results, as writing explicitly the analytical formulas for p_{sj} is actually very lengthy and does not clarify the physics much more here. We thus write for v_p the following:

$$\begin{aligned}v_p = \left.\frac{\delta v_{yp}}{k\psi_0 c_2}\right|_{M_1-1\ll 1} \cong{}& \frac{8(M_1-1)^3}{(\gamma+1)^2} \\ &+ \frac{(25-39\gamma)(M_1-1)^4}{(\gamma+1)^3} \\ &+ \frac{(71-190\gamma+123\gamma^2)(M_1-1)^5}{(\gamma+1)^4} + O[(M_1-1)^6].\end{aligned} \tag{50}$$

We can also express the tangential velocity in units of $k\psi_0 D$, which amounts to multiplying the above result by c_2/D,

$$\begin{aligned}\left.\frac{\delta v_{yp}}{k\psi_0 D}\right|_{M_1-1\ll 1} \cong{}& \frac{8(M_1-1)^3}{(\gamma+1)^2} \\ &+ \frac{(-31\gamma+1)(M_1-1)^4}{(\gamma+1)^3} \\ &+ \frac{4(17\gamma^2-8\gamma+7)(M_1-1)^5}{(\gamma+1)^5} \\ &+ O[(M_1-1)^6],\end{aligned} \tag{51}$$

or in units of $k\psi_0 U$, after multiplying Eq. (50) by c_2/U,

$$\begin{aligned}\left.\frac{\delta v_{yp}}{k\psi_0 U}\right|_{M_1-1\ll 1} \cong{}& \frac{2(M_1-1)^2}{\gamma+1} \\ &+ \frac{(-19\gamma+13)(M_1-1)^3}{4(\gamma+1)^2} \\ &+ \frac{47\gamma^2-146\gamma+63}{8(\gamma+1)^3}(M_1-1)^4 \\ &+ O[(M_1-1)^5].\end{aligned} \tag{52}$$

In Fig. 2 we have only shown the envelope of the above equation for $\gamma = 1$ with the velocity normalized with c_2. In Fig. 4 we show δv_{yp} in units of $k\psi_0 U$ for three different gases with γ equal to 7/5, 5/3, and 3. Weak shock asymptotic expansions [Eqs. (50)–(52)] are shown superposed to the exact curves.

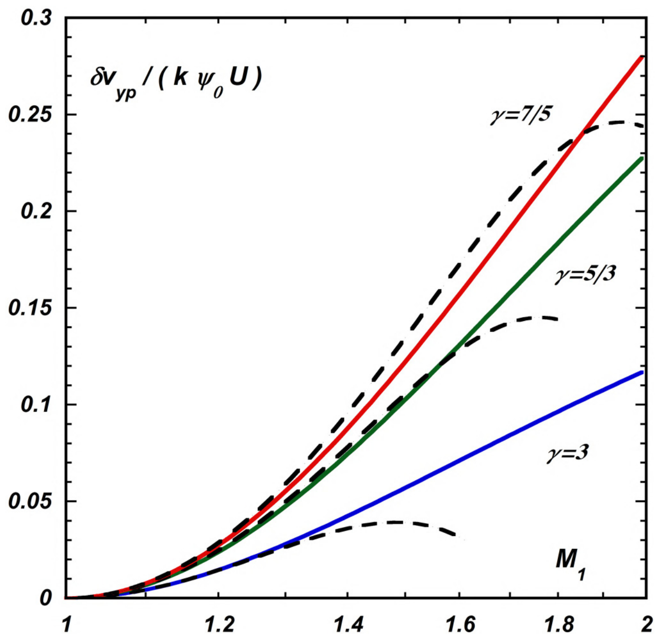

FIG. 4. (Color online) The tangential velocity δv_{yp} in units of $k\psi_0 U$ at the rigid piston surface when the shock is very far away as a function of the shock Mach number M_1 for different values of γ. The weak shock asymptotic from Eq. (52) is shown.

2. *Strong shock limit* ($M_1 \gg 1$)

In this other regime, the plots look apparently different depending on the normalization used. When using c_2 as a characteristic velocity, we see from the strong shock behavior that the curves tend to a constant for $M_1 \gg 1$, with the limiting value being a function of γ. If we use c_1 as the normalization velocity, the plots look like straight parallel lines in the double logarithmic plot. This means that the asymptotic velocity is proportional to the shock speed and the proportionality factor is a function of γ. In the ideal limit of $\gamma \to 1$, this factor equals unity. The limiting behavior for $\gamma = 1$ at very strong shocks can be easily inferred from Eq. (27). At first we note that for $\gamma \equiv 1$ and $M_1 \gg 1$ it is as follows:

$$\Omega \cong \frac{M_1^3}{2} + O\left(\frac{1}{M_1^2}\right),\qquad \sinh\chi_s \cong \frac{1}{M_1^2} + O\left(\frac{1}{M_1^3}\right). \tag{53}$$

The value of $\tilde{P}_s(q=\chi_s)$ needs to be obtained from the functional equation again. In this limit, we see that $\sinh\chi_s \approx 0$, hence it is enough to compute $\tilde{P}_s(0)$. The functions λ_1 and λ_2 must be evaluated at $\sinh q = 1/M_1$. Going back to Eq. (31) and expanding in powers of $1/M_1$ we obtain the following:

$$\lambda_1 \cong -\frac{4}{M_1},\qquad \lambda_2 \cong -1, \tag{54}$$

which gives, after substitution into Eq. (43),

$$\tilde{v}_p(\gamma = 1, M_1 \gg 1) \cong M_1. \tag{55}$$

For other realistic values of $\gamma > 1$, the asymptotic velocity at the piston is always proportional to D for strong shocks (typically for $M_1 > 3$). The proportionality factor depends on γ and can be calculated with an appropriate expansion in powers of $1/M_1$. We change the normalization velocity from c_2 to D and make an expansion in powers of $1/M_1$ for each factor that enters into the formula for $\tilde{v}_p$. Actually, it is enough to calculate the limiting values of these expressions in the limit $M_1 \gg 1$. We show each factor separately as follows:

$$\begin{aligned}\Omega &\cong \frac{\sqrt{2\gamma}}{(\gamma-1)^{3/2}} + O\left(\frac{1}{M_1^2}\right),\\ \sinh\chi_s &\cong \sqrt{\frac{\gamma-1}{\gamma+1}} + O\left(\frac{1}{M_1^2}\right),\\ \tilde{P}_s(\chi_s) &\cong -\frac{2(\gamma-1)(2\gamma^4+165\gamma^3-253\gamma^2+95\gamma-1)\sqrt{\gamma^2-1}}{(2\gamma-1)(\gamma^5+291\gamma^4-476\gamma^3+228\gamma^2-29\gamma+1)}.\end{aligned} \tag{56}$$

We show the strong shock limit of the tangential velocity at the piston, in units of $k\psi_0 c_2$, $k\psi_0 D$, and $k\psi_0 U$, respectively,

$$\left.\frac{\delta v_{yp}}{k\psi_0 c_2}\right|_{M_1\gg 1} \cong \frac{2(2\gamma^4+165\gamma^3-253\gamma^2+95\gamma-1)}{(2\gamma-1)(\gamma^5+291\gamma^4-476\gamma^3+228\gamma^2-29\gamma+1)}\sqrt{\frac{2\gamma}{\gamma-1}}, \tag{57}$$

$$\left.\frac{\delta v_{yp}}{k\psi_0 D}\right|_{M_1\gg 1} = \frac{4\gamma(2\gamma^4+165\gamma^3-253\gamma^2+95\gamma-1)}{(\gamma+1)(2\gamma-1)(\gamma^5+291\gamma^4-476\gamma^3+228\gamma^2-29\gamma+1)}, \tag{58}$$

$$\left.\frac{\delta v_{yp}}{k\psi_0 U}\right|_{M_1\gg 1} = \frac{2\gamma(2\gamma^4+165\gamma^3-253\gamma^2+95\gamma-1)}{(2\gamma-1)(\gamma^5+291\gamma^4-476\gamma^3+228\gamma^2-29\gamma+1)}. \tag{59}$$

In Fig. 5 we show $\delta v_{yp}/(k\psi_0 U)$ as a function of M_1 and the results are compared with the strong shock limits given in Eqs. (57)–(59).

B. Free surface

In this case, we require the vanishing of the piston pressure perturbations at any time. By looking at Eq. (12), we realize

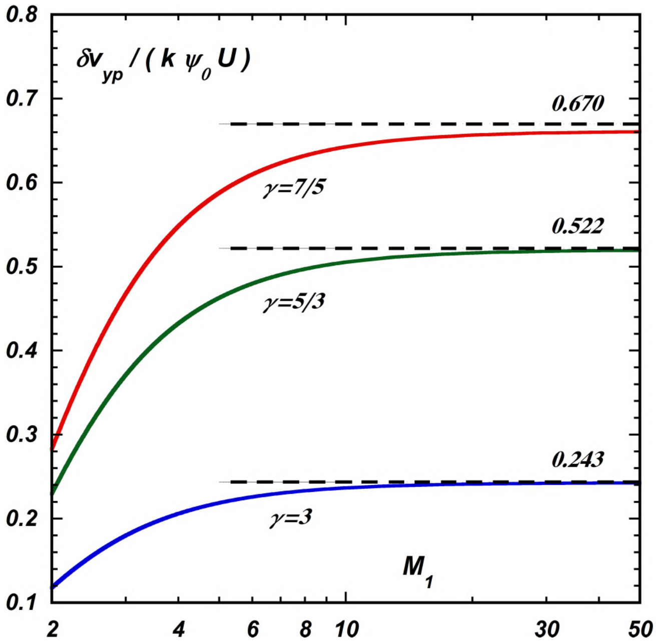

FIG. 5. (Color online) The tangential velocity δv_{yp} in units of $k\psi_0 U$ at the rigid piston surface when the shock is very far away as a function of the shock Mach number M_1 for different values of γ. The strong shock asymptotic from Eq. (59) is shown.

that the piston tangential velocity does not change in time and hence $\delta v_{yp} = \tilde{v}_{s0} k\psi_0 c_2$. Thus the boundary condition relating the normal and tangential velocities at the piston [Eq. (42)] now reads as follows:

$$u_p = \left.\frac{\delta v_{xp}}{k\psi_0 c_2}\right|_{\tau\to\infty} = \tilde{v}_{s0} + \Omega \sinh \chi_s \tilde{P}_s(q = \chi_s). \tag{60}$$

The value of $\tilde{P}_s$ has to be evaluated from Eq. (29) and the functions must be defined in Eq. (31). In Fig. 6 we plot the

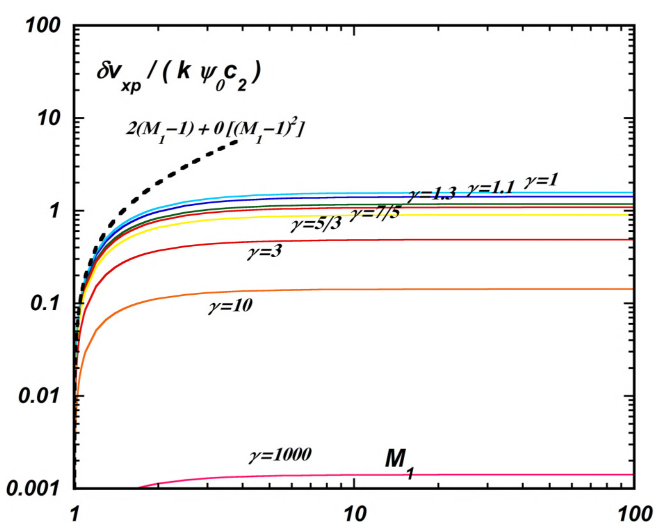

FIG. 6. (Color online) The normal velocity δv_{xp} at the rigid piston surface when the shock is very far away as a function of the shock Mach number M_1 for different values of γ. The perturbation velocity is normalized in units of $k\psi_0 c_2$.

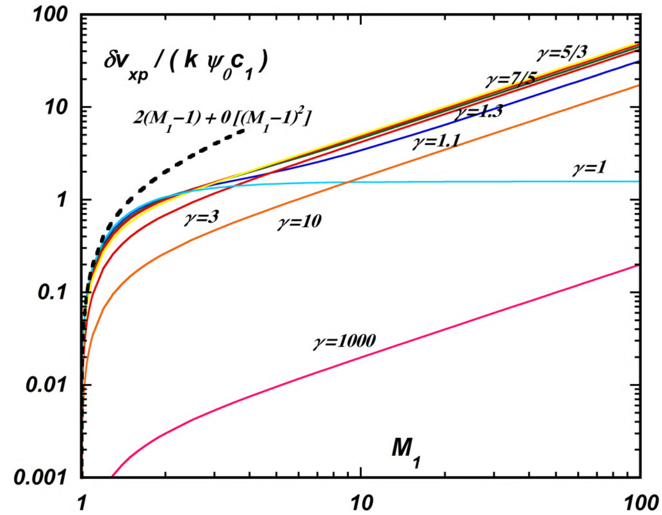

FIG. 7. (Color online) The normal velocity δv_{xp} at the rigid piston surface when the shock is very far away as a function of the shock Mach number M_1 for different values of γ. The perturbation velocity is normalized in units of $k\psi_0 c_1$.

value of u_p as a function of the shock Mach number M_1 for different values of the adiabatic exponent γ. The same is done in Fig. 7, but the normalization velocity used here is c_1 instead of c_2. Very high values of γ have been included as case studies in Figs. 6 and 7. Even though these values do not correspond to ideal gases, it is known that high values of γ are used to roughly model substances in liquid or solid state. At a given value of M_1, the dimensionless velocity $\delta v_{xp}/(k\psi_0 c_1)$ increases at first as γ decreases from higher values, reaching a maximum value at some lower γ to later decrease as $\gamma \to 1$. The curious result is that for the ideal case of $\gamma = 1$, the dimensionless asymptotic velocity tends to $\pi/2$ in the strong shock limit. This last result was derived for the first time in Ref. [18], when studying the physics of corrugated shocks driven by an ablation surface. Here we confirm that prediction in the limit of highly compressible fluids and very strong shocks. To reach this limit, the number of terms used in Eq. (29) is very high, above 100 terms inside the summation, and the number increases further as M_1 is increased. For this particular case, the solution found for the functional equation is very slowly convergent, as high-order shifts are needed to increase accuracy. This is due to the fact that in the ideal case of $\gamma \cong 1$ and $M_1 \gg 1$, the shock and the piston travel essentially at the same speed and it may take an almost infinite amount of time for the shock to separate from the piston. Hence all the infinite reverberations are important to describe the pressure field between both surfaces. This is mathematically equivalent to include higher and higher-order shifts in multiples of $2\chi_s$ inside the arguments of the functions λ_1 and λ_2. As discussed for the rigid piston situation, a similar dimensional analysis leads us from the scaling shown in Fig. 6 to Fig. 7. It is enough to change δv_{yp} for δv_{xp}. In the strong shock limit we get, from Fig. 6 the scaling

$$\left.\frac{\delta v_{xp}}{c_2}\right|_{\tau\to\infty} \propto g_2(\gamma) \tag{61}$$

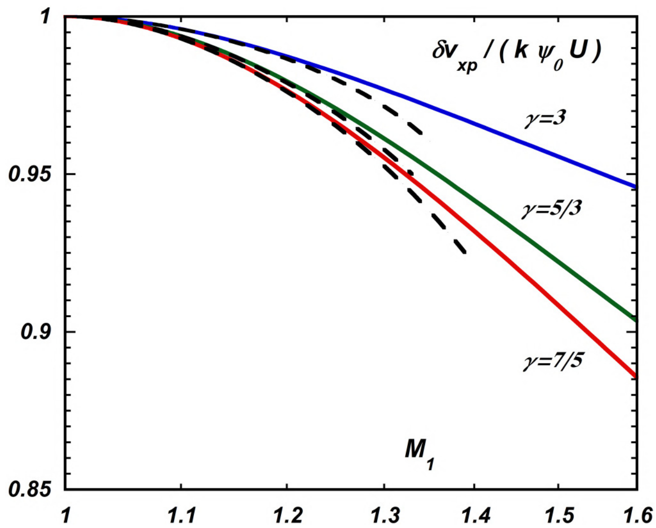

FIG. 8. (Color online) Normal velocity perturbation at the free piston surface in units of $k\psi_0 U$ for three different values of γ (7/5, 5/3, and 3) as a function of the shock Mach number M_1. Also shown are the asymptotic limits for weak shocks as explained in the text.

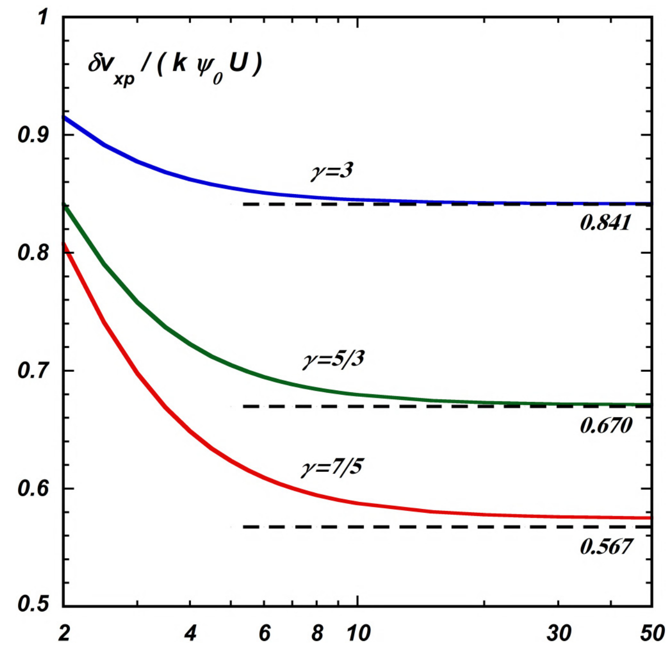

FIG. 9. (Color online) Normal velocity perturbation at the free piston surface in units of $k\psi_0 U$ for three different values of γ (7/5, 5/3, and 3) as a function of the shock Mach number M_1. Also shown are the asymptotic limits for strong shocks as explained in the text.

for some dimensionless function g_2. As $c_2 \propto M_1 c_1$ in the strong shock limit, it follows the proportionality seen in Fig. 7 in the strong shock regime. When $\gamma = 1$, the independence of δv_{xp} on $M_1 \gg 1$ follows directly from Eq. (61) and the fact that $c_2 = c_1$ as deduced from Eq. (3).

As we have done in the previous subsection, we now discuss the limit of weak shocks.

1. *Weak shock regime* ($M_1 - 1 \ll 1$)

For very weak shocks, we use the same scalings as in Eq. (53). However, $\tilde{P}_s(q = \chi_s)$ has a different behavior with respect to γ and M_1. The values of $\tilde{p}_{s1}$, $\tilde{p}_{s3}$, and $\tilde{p}_{s5}$ for this case are calculated from the corresponding functional equation for the shock pressure perturbations in the free surface case (Figs. 8 and 9). We expand them in powers of $M_1 - 1$, use the formulas shown in Eq. (49), and substitute into Eq. (60) and write the following:

$$u_p(M_1 - 1 \ll 1) = \left.\frac{\delta v_{xp}}{k\psi_0 c_2}\right|_{M_1-1\ll 1} \cong \frac{4(M_1-1)}{\gamma+1} + \frac{(-10\gamma+6)(M_1-1)^2}{(\gamma+1)^2} + \frac{(26\gamma^2 - 36\gamma + 2)(M_1-1)^3}{3(\gamma+1)^3} + O[(M_1-1)^4]. \quad (62)$$

We also show the expansion for the same velocity but in units of $k\psi_0 D$ as follows:

$$\left.\frac{\delta v_{xp}}{k\psi_0 D}\right|_{M_1-1\ll 1} \cong \frac{4(M_1-1)}{\gamma+1} - \frac{6(M_1-1)^2}{\gamma+1} + \frac{8\gamma(M_1-1)^3}{(\gamma+1)^2} + O[(M_1-1)^4]. \quad (63)$$

This scaling differs from the scaling found in the weak shock limit of the rigid piston for the tangential velocity. From Eq. (62), we see that the normal velocity is proportional to the fluid velocity $M_1 - 1$, for very weak shocks, as does the compressed fluid velocity in that limit. Therefore, it may be useful to rewrite the previous formula using U as the normalization velocity. From the above equation, after multiplying by c_2/U and expanding up to third order, we obtain the following:

$$\left.\frac{\delta v_{xp}}{k\psi_0 U}\right|_{M_1-1\ll 1} \cong 1 - \frac{2(M_1-1)^2}{3(\gamma+1)} + O[(M_1-1)^3]. \quad (64)$$

We see that all the curves start from unity at $M_1 = 1$, which means that for weak shocks it is $\delta v_{xp} \cong k\psi_0 U$ and the approximation is not too bad up to shocks of moderate strength. The scaling changes drastically for very strong shocks, similarly to what happened with the tangential velocity for the rigid piston situation. As the shock strength increases, the normal velocity perturbation is no longer proportional to U but becomes proportional to D. This behavior is shown in the following subsection.

2. *Strong shock regime* ($M_1 \gg 1$)

We proceed similarly as with the rigid piston. We only need to calculate the corresponding value for $\tilde{P}_s(q = \chi_s)$. We get the following:

$$\tilde{P}_s(\chi_s) \cong -\frac{\sqrt{\gamma^2-1}}{\gamma(2\gamma+1)} \times \frac{122\gamma^4 - 227\gamma^3 + 139\gamma^2 - 25\gamma - 1}{144\gamma^4 - 239\gamma^3 + 115\gamma^2 - 13\gamma + 1}. \quad (65)$$

We use Ω and $\sinh\chi_s$ from Eq. (56). The asymptotic value of the initial tangential velocity is $\tilde{v}_{s0} \cong \sqrt{2/[\gamma(\gamma-1)]}$. Collecting these results together, we obtain the desired asymptotic limit as follows:

$$\left.\frac{\delta v_{xp}}{k\psi_0 c_2}\right|_{M_1\gg 1} \cong \frac{8(3\gamma-1)(12\gamma^2-15\gamma+5)\sqrt{2\gamma(\gamma-1)}}{(2\gamma-1)(144\gamma^4-239\gamma^3+115\gamma^2-13\gamma+1)}. \tag{66}$$

The previous expansion of the velocity δv_{xp} can also be expressed in units of $k\psi_0 D$ as follows:

$$\left.\frac{\delta v_{xp}}{k\psi_0 D}\right|_{M_1\gg 1} \cong \frac{16\gamma(\gamma-1)(3\gamma-1)(12\gamma^2-15\gamma+5)}{(\gamma+1)(2\gamma-1)(144\gamma^4-239\gamma^3+115\gamma^2-13\gamma+1)}, \tag{67}$$

or, in units of $k\psi_0 U$,

$$\left.\frac{\delta v_{xp}}{k\psi_0 U}\right|_{M_1\gg 1} \cong \frac{8\gamma(\gamma-1)(3\gamma-1)(12\gamma^2-15\gamma+5)}{(2\gamma-1)(144\gamma^4-239\gamma^3+115\gamma^2-13\gamma+1)}. \tag{68}$$

IV. ASYMPTOTIC VELOCITIES: APPROXIMATE FORMULA FOR ANY SHOCK STRENGTH

In the previous section we have shown the asymptotic limits of the piston velocities either for rigid or free surfaces in the limits of weak and strong shocks. The main conclusion of Sec. II is that at any surface driving a corrugated shock, asymptotically in time, normal and/or tangential velocity perturbations develop on it. These velocities are, in some cases, accessible to experimental measurement or numerical calculation, which makes them an exquisite tool with which to test the theoretical models used to describe the particular problem under study. Therefore, they become an important quantity for research in the domain of HEDP. This is the main reason why analytical models that study hydrodynamic perturbations from first principles, like the calculations shown here, are relevant. In Sec. II we have arrived at the conclusion that the normal and tangential velocity components at the piston are always related in the way shown in Eq. (42). This is the unique boundary condition to be asked at any "passive" surface like the piston in the problems considered here. The relationship between δv_{xp} and δv_{yp} expressed in Eq. (42) is not trivial and not evident *a priori*. In fact, we have had to develop the whole perturbation theory for the shock and the downstream profiles in order to arrive at it. Equation (42) is the only correct boundary condition to be applied at any "passive" surface driving a shock if we want to successfully calculate those velocities in any range of shock strengths or fluid compressibilities. In this work, we have concentrated on a single fluid, inside which a single shock is moving, as the calculations are simpler and serve as a starting step to the more complex problem of two fluids. The weak shock expansions shown in Eqs. (50)–(52) for the rigid piston case and Eqs. (62)–(64) for the free surface case are valid for Mach numbers below approximately 1.4. To go further we would need a larger number of coefficients ($\tilde{p}_{s7}$, etc.) inside the expression of $\tilde{P}_s(\chi_s)$, which makes this expansion not practical for $M_1 > 1.4$ and it probably could not go much beyond that. On the opposite side, for very large Mach numbers, we have obtained the limiting values of the velocities, which are functions of γ, as given in Eqs. (57)–(59) for the rigid piston and Eqs. (66)–(68) for the free surface problem. The question that remains to be answered is as follows: What can we say for the range of moderate strength shocks, that is, inside the very important interval $1.4 < M_1 < \infty$. Interpolating between the asymptotic expansions certainly could be a way, but the formulas so obtained might not respect the physics that underlies the perturbation dynamics in that range. Fortunately, the function [Eq. (34)] suggested in Sec. II is a very good estimate for the shock pressure function $\tilde{P}_s$ for not very compressible gases at any M_1 value. This requires us to use $\gamma > 1.1$ as a constraint. If we want to study lower values of γ, more iterations should be performed. Therefore, we can write approximate and accurate formulas for the asymptotic velocities under these restrictions. We have, for the rigid piston tangential velocity at the piston,

$$\frac{\delta v_{yp}}{k\psi_0 c_2} = -\Omega\sinh\chi_s\left\{\lambda_1(\chi_s)+\lambda_2(\chi_s)\left[\frac{\lambda_1(3\chi_s)}{1-\lambda_2(3\chi_s)}\right]\right\}, \tag{69}$$

where $\lambda_1(q)$ and $\lambda_2(q)$ for the rigid piston case are given in Eqs. (28). For the free surface, the approximate expression for the asymptotic normal velocity at the piston is given by the following:

$$\frac{\delta v_{xp}}{k\psi_0 c_2} = \tilde{v}_{s0} + \Omega\sinh\chi_s\left\{\lambda_1(\chi_s)+\lambda_2(\chi_s)\left[\frac{\lambda_1(3\chi_s)}{1-\lambda_2(3\chi_s)}\right]\right\}, \tag{70}$$

where $\tilde{v}_{s0} = \delta v_{ys}(0+)/(k\psi_0 c_2)$ is the dimensionless initial tangential velocity created between the shock and the piston at $t = 0+$. The functions $\lambda_1(q)$ and $\lambda_2(q)$ that enter the last equation for the free surface case are given in Eq. (31). In Fig. 10 we compare the predictions of Eq. (69) with the exact result for the rigid piston case for three values of γ. The same is done with Eq. (70) for the free surface case in Fig. 11. To summarize the discussion of the past two sections, we may add that the results of the expansions of Sec. III are easy to use, without any sophisticated software, and could be ideally implemented with a pocket calculator, when needed, as they involve polynomial expressions in $M_1 - 1$, or $1/M_1$, and rational expressions of γ. However, the approximate formulas given in Eqs. (69) and (70) need at least a symbolic software like MATHEMATICA or MAPLE in order to define all the quantities given in Sec. II, as a function of shock strength M_1 and fluid

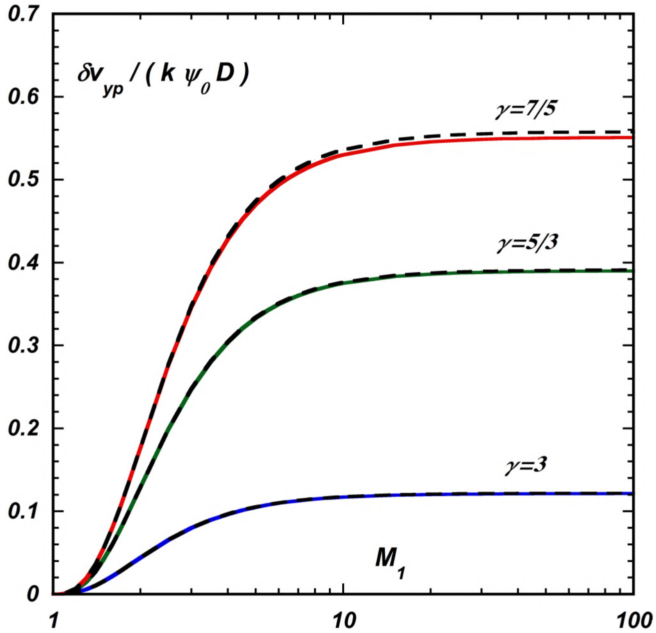

FIG. 10. (Color online) Comparison of the exact and approximate values [according to Eq. (69)] of the piston tangential velocity perturbation as a function of the shock Mach number.

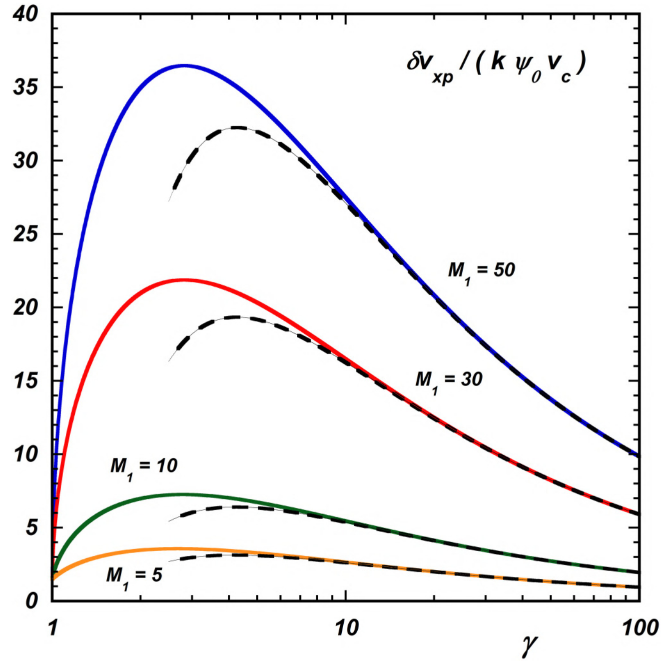

FIG. 12. (Color online) Normal velocity perturbation at the piston normalized with v_c as a function of γ for different values of M_1.

isentropic exponent γ in order to define the functions λ_1 and λ_2, which is necessary to get the asymptotic velocities.

V. FREE SURFACE NORMAL VELOCITY DEPENDENCE ON γ

To see the absolute dependence of δv_{xp} on γ, we show the normal velocity in units of $v_c k\psi_0$, where the characteristic

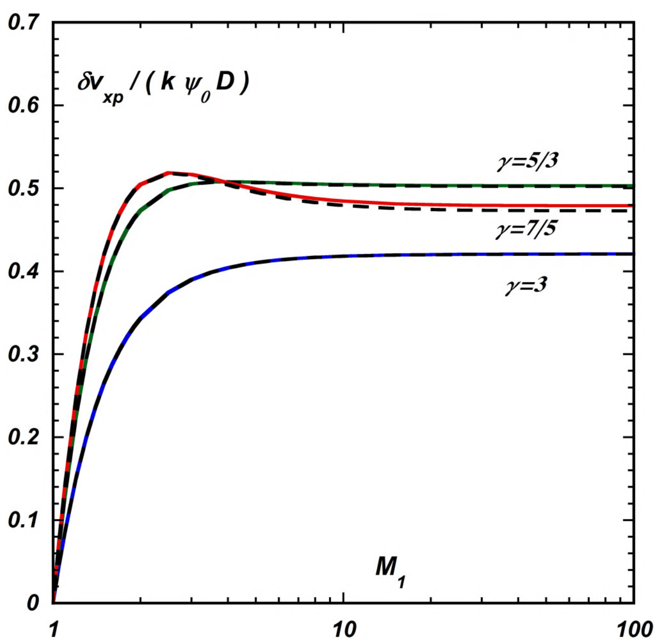

FIG. 11. (Color online) Comparison of the exact and approximate values [according to Eq. (70)] of the free surface normal velocity perturbation as a function of the shock Mach number.

velocity $v_c = \sqrt{p_1/\rho_1}$, in Fig. 12. In this way, there is no dependence on γ for the factor we use to normalize the perturbation velocity. We see in Fig. 12 that at any given value of M_1 the normal velocity reaches a maximum value for some value of the isentropic exponent which we indicate with γ_m. We also show the curves (dashed) that represent the asymptotic expansion of $\delta v_{xp}/(k\psi_0 v_c)$ in powers of $1/\gamma$. This expansion is given in Eq. 71 as follows:

$$\left.\frac{\delta v_{xp}}{k\psi_0 v_c}\right|_{\gamma\gg 1} \cong \frac{2\left(M_1^2-1\right)}{M_1}\frac{1}{\gamma^{1/2}} + \frac{1}{-72M_1^{11}+84M_1^9-32M_1^7+4M_1^5} \times \left(205M_1^{12}-559M_1^{10}+628M_1^8-390M_1^6 + 141M_1^4-27M_1^2+2\right)\frac{1}{\gamma^{3/2}}. \tag{71}$$

In Fig. 13 we show the dependence of γ_m on M_1. We note that there is a maximum value for γ_m, equal to $\gamma_m^{\max} = 2.822\ldots$, reached at $M_1 \gg 1$. In Fig. 14 we show the maximum value of the normal velocity perturbation (δv_{xpm}), achieved only at $\gamma = \gamma_m$ as a function of M_1. The curious result, not obvious from the equations used to obtain it, is that δv_{xpm} scales linearly for almost any value of $M_1 > 1$, except perhaps very near $M_1 = 1$. The dashed line in Fig. 14 satisfies $\delta v_{xpm} \sim 0.724\ M_1$. For a given shock Mach number, this is the maximum attainable perturbation velocity at the piston and for any other fluid with $\gamma \neq \gamma_m$, and the piston velocity perturbation would be smaller than the value predicted from Fig. 14.

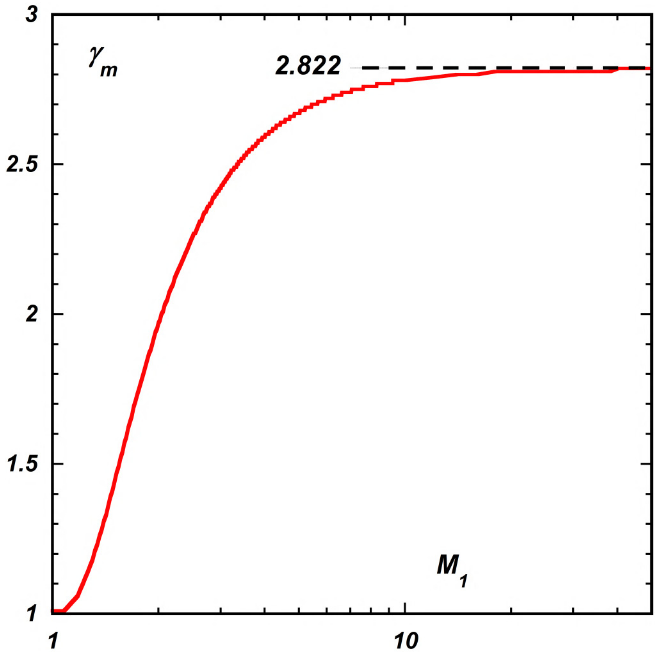

FIG. 13. (Color online) Value γ_m of the isentropic exponent for which the normal velocity perturbation at the piston is the maximum possible at the given shock Mach number M_1.

VI. SUMMARY

We have presented an analytic model to study the linear RM-like flow that develops between a corrugated shock and the piston driving it. Rigid and free surface conditions were imposed at the left piston surface. Even though the solution to the wave equation is independent of the equation of state, the results shown here consider an ideal gas but are not limited in principle with this constraint. The asymptotic velocities that develop between both surfaces are strongly dominated by the vorticity generated at the shock during the whole time evolution, which is dependent on the shock pressure perturbations. In the reference frame of the compressed fluid, these velocity fields are steady state and the perturbations at the piston reach an asymptotic value when the shock is far enough. The accurate determination of these velocities (either tangential or normal to the piston surface) is an important diagnostic tool, useful for the design of numerical or real experiments. The results and the method of calculation developed here constitute the first step of more complex calculations aimed at deriving explicit analytical expressions for the classical two-fluid RM instability problem. The main mathematical difficulty to get the asymptotic velocities at an arbitrary shock strength or fluid compressibility is represented by the mathematical complexities of the functional equation for the shock pressure fluctuations. We cannot avoid dealing with Eq. (27). It has the information of the perturbation fields (pressure, velocities, densities, etc.) in the whole space between the shock and the piston. For all these years we have been unable to find a closed-form expression for the solution of that equation and this is the reason why we have to rely either on approximate expansions at some physical limits (weak or strong as in Sec. III) or to devise an approximate formula that describes the whole interval ($1 \leqslant M_1 < \infty$) in some restricted domain of the isentropic exponent γ. In fact, in Sec. IV we see that iterating once on the functional equation allows us to get at least two-digit accuracy for shocks of arbitrary strength if we stay above $\gamma > 1.1$. As we approach the high compressibility limit ($M_1 > 5$, $\gamma - 1 \ll 1$), the shock takes a longer time to reach its asymptotic planarity and its ripple makes more oscillations which in turn are responsible for generating larger vorticity. Equivalently, we could say that sound-wave production becomes very important as the shock Mach number increases and the interaction with the piston surface lasts for a longer time. The effect of this prolonged interaction is in the final values of the tangential or normal velocities at the piston, depending on the piston boundary condition. The advantage of the results of Sec. III is that those expansions can be easily calculated without any sophistication in mathematical software. The disadvantage of those results is that they are limited to $M_1 < 1.4$. The best strategy we have found for the interval $M_1 > 1.4$ is to use the results of Eqs. (69) and (70). The agreement between the exact solution and the approximate ones is very good for almost any shock Mach number if γ is not very near unity, as can be seen in Figs. 10 and 11. From dimensional arguments, the scaling $\delta v_{xp},\delta v_{yp} \sim D$ can be seen in the strong shock limit for both piston boundary conditions. For weak shocks, the useful scaling $\delta v_{xp} \sim U$ is noteworthy in the free surface problem. Finally, we show here two additional plots, for the rigid and free surfaces, respectively. In the horizontal axis we plot the asymptotic velocity at the piston in units of the shock speed and in the vertical axis we plot the same velocity but in units of the compressed fluid velocity. These figures have curious shapes and reveal in qualitative form the complex behavior of the asymptotic velocities as a function of the shock Mach number. In Fig. 15 we show this for the tangential velocity at the piston

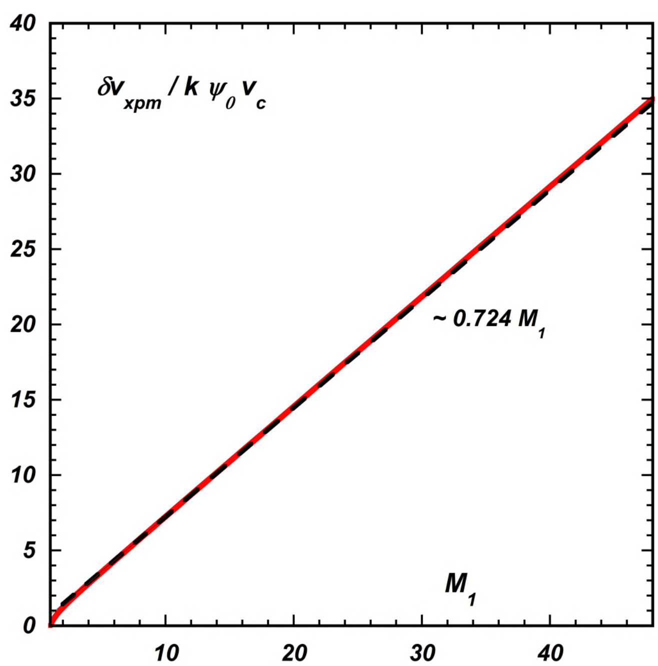

FIG. 14. (Color online) Maximum value of the normal velocity perturbation at the piston, reached at $\gamma = \gamma_m$, as a function of the shock Mach number M_1.

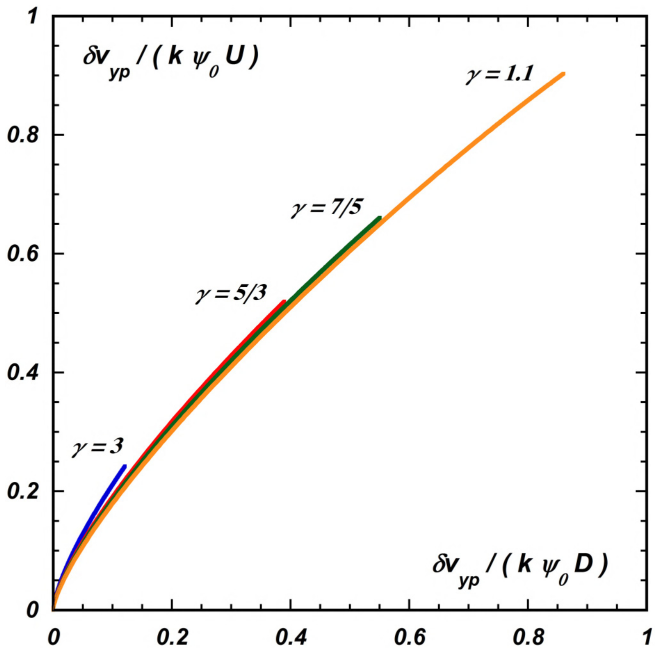

FIG. 15. (Color online) Exact tangential asymptotic velocity at the rigid piston for different ideal gases. The horizontal axis is scaled with the shock speed and the vertical axis is normalized with the compressed fluid velocity.

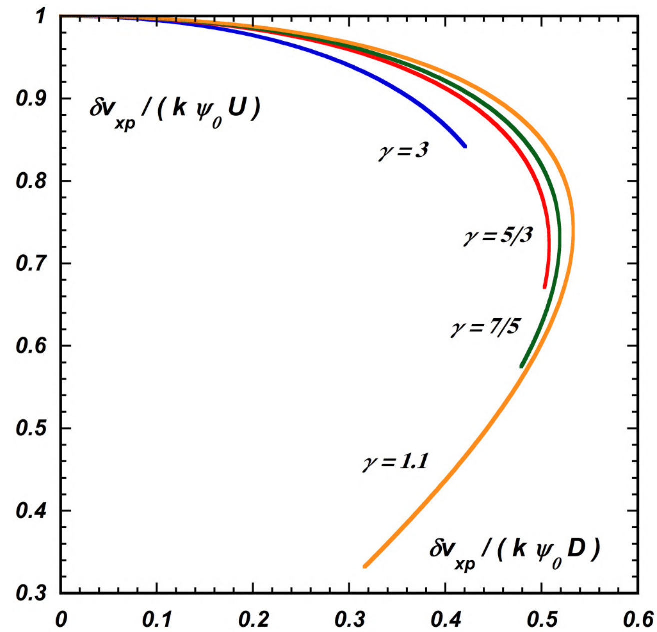

FIG. 16. (Color online) Exact normal asymptotic velocity at the free surface for different ideal gases. The horizontal axis is scaled with the shock speed and the vertical axis is normalized with the compressed fluid velocity.

and all the curves practically overlap each other for the range of γ values studied. The weak shock limit starts at the point with coordinates (0,0) and the very strong shock limit asymptotic is the ending point of each curve. In the plots shown here, $M_1 = 100$ was used, which was considered enough to reach the high-compression limit. The same is shown in Fig. 16. The weak shock limit here corresponds to the point with coordinates (0,1). All the curves start practically together and separate when $M_1 > 1.4$ and show a distinctive behavior as compared to the rigid piston in the strong shock limit.

The results shown here are preliminary calculations before studying the standard RM instability with two fluids in order to obtain useful and accurate analytical expressions for shocks of arbitrary strength and fluids with arbitrary compressibility.

ACKNOWLEDGMENTS

The authors thank A. R. Piriz and A. Bret (UCLM) for encouragement and support. In particular, thanks are given to A. R. Piriz for discussions about the strong shock limit behavior. J.G.W. thanks T. Sano from Osaka University for encouraging discussions. F.C.C. acknowledges support from INEI (UCLM). The authors of this work received support from MINECO under Grant No. ENE2013-45661-C2-1-P and from JCCM Grant No. PEI11-0056-1890.

[1] J. N. Johnson and R. Cheret, *Classic Papers in Shock Compression Science* (Springer, New York, 1998).
[2] A. E. Roberts, Los Alamos Scientific National Laboratory Report No. LA-299 (unpublished). See National Technical Information Service Document No. PB2004-100597.
[3] R. D. Richtmyer, Commun. Pure Appl. Math. **13**, 297 (1960).
[4] E. E. Meshkov, Fluid Dyn. **4**, 101 (1969).
[5] M. G. Briscoe and A. A. Kovitz, J. Fluid Mech. **31**, 529 (1968).
[6] A. L. Velikovich, J. P. Dahlburg, A. J. Schmitt, J. H. Gardner, L. P. Phillips, F. L. Cochran, Y. K. Chong, G. Dimonte, and N. Metzler, Phys. Plasmas **7**, 1662 (2000).
[7] A. R. Piriz, J. J. Lopez Cela, N. A. Tahir, and D. H. H. Hoffmann, Phys. Rev. E **74**, 037301 (2006).
[8] A. R. Piriz, J. J. Lopez Cela, N. A. Tahir, and D. H. H. Hoffmann, Phys. Rev. E **78**, 056401 (2008).
[9] G. Dimonte, G. Terrones, F. J. Cherne, T. C. Germann, V. Dupont, K. Kadau, W. T. Buttler, D. M. Oro, C. Morris, and D. L. Preston, Phys. Rev. Lett. **107**, 264502 (2011).
[10] G. H. Miller and T. J. Ahrens, Rev. Mod. Phys. **63**, 919 (1991).
[11] S. I. Abarzhi, Phys. Scr. T **132**, 014012 (2008).
[12] M. Herrmann, P. Moin, and S. I. Abarzhi, J. Fluid Mech. **612**, 311 (2008).
[13] A. L. Velikovich, M. Herrmann, and S. I. Abarzhi, J. Fluid Mech. **751**, 432 (2014).
[14] G. Fraley, Phys. Fluids **29**, 376 (1986).
[15] J. G. Wouchuk and K. Nishihara, Phys. Plasmas **4**, 1028 (1997).
[16] J. G. Wouchuk, Phys. Rev. E **63**, 056303 (2001).
[17] A. L. Velikovich, Phys. Fluids **8**, 1666 (1996).
[18] V. N. Goncharov, O. V. Gotchev, E. Vianello, T. R. Boehly, J. P. Knauer, P. W. McKenty, P. B. Radha, S. P. Regan, T. C. Sangster, S. Skupsky, V. A. Smalyuk, and R. Betti, Phys. Plasmas **13**, 012702 (2006).

[19] L. D. Landau and E. M. Lifshitz, *Fluid Mechanics*, 2nd ed. (Butterworth-Heinemann, Oxford, 2000).
[20] J. G. Wouchuk, C. Huete Ruiz de Lira, and A. L. Velikovich, Phys. Rev. E **79**, 066315 (2009).
[21] P. M. Zaidel, J. Appl. Math. Mech. **24**, 316 (1960).
[22] A. L. Velikovich, J. G. Wouchuk, C. Huete Ruiz de Lira, N. Metzler, S. Zalesak, and A. J. Schmitt, Phys. Plasmas **14**, 072706 (2007).
[23] J. G. Wochuk and J. López Cavada, Phys. Rev. E **70**, 046303 (2004).
[24] Y. Yang, Q. Zhang, and D. H. Sharp, Phys. Fluids **6**, 1856 (1994).
[25] C. Huete Ruiz de Lira, A. L. Velikovich, and J. G. Wouchuk, Phys. Rev. E **83**, 056320 (2011).
[26] C. Huete, J. G. Wouchuk, and A. L. Velikovich, Phys. Rev. E **85**, 026312 (2012).
[27] C. Huete, J. G. Wouchuk, B. Canaud, and A. L. Velikovich, J. Fluid Mech. **700**, 214 (2012).
[28] G. I. Barenblatt, *Scaling, Self-Similarity, and Intermediate Asymptotics*, 1st ed. (Cambridge University Press, New York, 1996).